ISSN 0018-1439, High Energy Chemistry, 2024, Vol. 58, Suppl. 4, pp. S528–S542. © Pleiades Publishing, Ltd., 2024.

# Machine Learning-assisted Study of Low-, Medium-, and High-Entropy Hydrogen Storage Alloys Validated by the Experimental Data

**T. R. Somo[a], M. V. Lototskyy[a, b], M. W. Davids[a], S. Nyallang Nyamsi[a], B. P. Tarasov[b, *], and S. Pasupathi[a]**

[a] *University of the Western Cape, HySA Systems Centre of Competence, Belville, 7535 South Africa*

[b] *Federal Research Center of Problems of Chemical Physics and Medicinal Chemistry, Russian Academy of Sciences, Chernogolovka, Moscow oblast, 142432 Russia*

**e-mail: tarasov@icp.ac.ru*

Received September 12, 2024; revised September 12, 2024; accepted September 20, 2024

**Abstract**—Advancing of hydrogen and metal hydride energy technologies requires purposeful development of efficient hydrogen storage materials, particularly, tuning their composition towards optimization of hydrogen sorption properties suitable for the end-use applications. This study employed linear regression modelling to analyze hydrogen storage properties of low-, medium- and high-entropy alloys with BCC, C14- and C15-$AB_2$ and $AB_5$ structures found in the literature (>350 entries in total) and to make predictions based on the model further validated by additional reference data and results of own experiments. It was found that the applied model gives a good qualitative correspondence with the reference data on hydrogen sorption capacity and thermodynamics of hydrogen interaction with the alloys but has a limiting predicting capacity allowing only rough quantitative estimations. It was also concluded that the unit cell volume, valence electron concentration, and, to a lesser extent, electronegativity mismatch, exhibit strong effects on the hydrogen sorption properties of the studied alloys while the influence of other factors including the mixing entropy is much less pronounced.

**Keywords:** hydrogen storage materials, high entropy alloys, machine learning, linear regression

**DOI:** 10.1134/S0018143924701601

## THEORETICAL ANALYSIS

### *Introduction*

For over several decades, hydrogen has been investigated as the most promising clean and abundantly available alternative energy carrier. However, low density of hydrogen, high energy consumption of physical methods of its densification along with safety concerns pose numerous challenging problems. Therefore, looking for the efficient and safe solutions of hydrogen handling, particularly, its storage, remains in the focus of R&D activities worldwide [1–3].

Materials-based hydrogen storage including the use of (inter)metallic hydrides (MH) is the most promising way of the solution of above problems [4–6]. The use of MHs is especially efficient due to high volumetric storage density, as well as moderate operating temperatures, hydrogen pressures and consumption of energy taken in the form of low-grade heat [7, 8]. Additional competitive advantage of MH technologies as compared to the alternative hydrogen handling solutions includes their flexibility originated from the possibility of variation of hydrogen sorption properties in exceptionally wide limits by the variation of composition of the host multi-component hydrogen storage alloy [9].

Over the years, several classes of binary and multicomponent metal alloys have been studied for hydrogen storage and related applications. These include TiFe and its derivatives [8], Laves phase intermetallics [10], alloys with body–centered cubic (BCC) structure, e.g., Ti–V–Cr [11], and $AB_5$ intermetallics crystallized in $CaCu_5$-type structure, such as $LaNi_5$ [12]. The entropy of mixing ($\Delta S_{mix}$) in binary and ternary alloys of these types usually ranges from the low ($\Delta S_{mix} \le R$ where $R = 8.314$ J K$^{-1}$ mol$^{-1}$ is the universal gas constant) to the medium one ($R < \Delta S_{mix} \le 1.5R$). The increase of the mixing entropy above $\Delta S_{mix} = 1.5R$, i.e., passing from low- (LEA) and medium- (MEA) entropy alloys to the high-entropy (HEA) ones, has been considered as a way for further improvement of performance of hydrogen storage alloys. Previous reports have associated high entropy of mixing in HEAs with increased $H_2$ capacity [13, 14]. Additionally, it is believed that since hydrogen storage properties are composition-dependent, the wide compositional field of multicomponent alloys could provide an opportunity to design alloy compositions with

optimized hydrogen storage properties for each specific application [15]. Lastly, lattice distortion associated with HEAs resulting from mixing elements with different atomic sizes, creates better pathways for hydrogen diffusion [13].

In our recent work [16], we analyzed hydrogen storage performances of LEAs, MEAs and HEAs (BCC and $AB_2$-types), as related to their composition-related parameters including atomic size mismatch, valence electron concentration (VEC), as well as mixing entropy and enthalpy. This was done by statistical analysis of the effect of these parameters on the enthalpy of hydride formation and H/M ratio. It was shown that VEC exhibits the most significant effect while no clear correlations of H/M or enthalpy of hydride formation with electronegativity and atomic size mismatch, as well as $\Delta S_{mix}$, were observed. At the same time, the best correlations were obtained when the following six key properties of the alloys were accounted simultaneously:

- VEC;
- Unit cell volume per metal atom;
- The mixing enthalpies of the starting and hydrogenated alloy;
- Electronegativity mismatch;
- Size mismatch and
- Mixing entropy of the alloy.

Due to complexity of the high entropy alloys, much attention has been paid to computational simulation studies based on DFT calculations as well as machine learning to theoretically establish better understanding of the design and applications related to these materials. While the DFT simulations are characterized by time-consuming cycles, low efficiency and high costs, the machine learning methods provide effective data processing and strong prediction performance coupled with high accuracy, low computational cost facilitated by open access software and short processing periods, and thus been widely used in materials science [17–19]. Rahnama et al. [17] successfully used supervised machine learning to analyze database provided by the US Department of Energy on hydrides for hydrogen storage and different features for determining hydrogen storage capacity referred to as hydrogen weight percent. These features were ranked according to their importance. Ahmed and Siegel [20] predicted the hydrogen storage capacities of nearly million metal organic frameworks (MOFs) using machine learning. The predictions span a diverse collection of MOFs sourced from 19 databases and reveal performance under two operating conditions: pressure swing and temperature + pressure swing. Suwarno et al. [19] investigated the effect of alloying elements on the hydrogen storage properties of $AB_2$ alloys, i.e., the enthalpy of formation ($\Delta H$), phase abundance, and hydrogen capacity using machine learning. Their database comprised of 314 entries collected from the literature; the reference information included chemical compositions and hydrogen storage properties of the alloys.

In this study, the simplest machine learning algorithm, linear regression analysis, was applied to predict storage capacity and thermodynamic properties of multicomponent or multi-principal element alloys, including the standard Gibbs free energy ($\Delta G_H^\circ$) and temperature ($T_H$) at equilibrium $H_2$ pressure equal to 1 atm = 0.101325 MPa, or at $\Delta G_H^\circ = 0$. The used reference data were published between 2006 and 2023. The model relates the hydrogen storage properties to a set of the composition-derived key properties (input parameters) and the above-mentioned hydrogen storage characteristics (response values). This model aims to predict hydrogen storage properties of the alloys using a combination of the input parameters and subsequently provides better pathways for the experimental studies.

### *Classification of Multiprincipal Component Alloys and their Key Properties*

Main property which determines classification of multi-principal component alloys is the entropy of mixing ($\Delta S_{\text{mix}}$) of their components.

The entropy of mixing is mainly defined by a configurational term which is calculated as [21, 22]:

$$\Delta S_{\text{mix}} = -R\sum_{i=1}^{N}(C_i \ln C_i), \quad (1)$$

where $C_i$ is the atomic fraction of the $i$-th component in the $N$-component alloy.

Equation (1) is valid for the liquid or disordered solid phase with a random distribution of the alloy components on the lattice sites. For the ordered phases with several substructures, the mixing entropy can be calculated as [23]:

$$\Delta S'_{\text{mix}} = -R\sum_{s=1}^{k}\frac{a_s}{\left(\sum_{s=1}^{k} a_s\right)}\sum_{i=1}^{n}\left(C_i^s \ln C_i^s\right), \quad (2)$$

where $a_s$ is the number of the sites in the $s$ sublattice and $C_i^s$ relates to the fraction of the $i$-th component in the $s$ sublattice. Equation (2) assumes a random distribution of the alloy components on the sublattices. We note that such a random distribution is generally not a case, in particular, for the A- and B-sites of the $AB_{2\pm x}$ Laves type phases [24]. Taking into account Eq. (2), the value of the excess entropy of intermetallic HEAs may be noticeably higher than the one that could be calculated by using conventional Eq. (1).

The entropy of mixing is an important factor which is related to the ordering of the metal atoms in the crystal lattice of a single-phase alloy and can affect

various alloy properties. Depending on the value of the mixing entropy, the alloys are classified into three groups: low- (LEA; $\Delta S_{mix} \le R$), medium- (MEA; $R < \Delta S_{mix} \le 1.5R$) and high-entropy (HEA; $\Delta S_{mix} > 1.5\ R$) alloys [25, 26].

Another key property is the enthalpy of mixing ($\Delta H_{mix}$). For an $N$-component alloy, $\Delta H_{mix}$ can be calculated using the regular melt model starting from the concentrations ($C$) taken in atomic fractions and enthalpies of mixing of the $i$-th and $j$-th alloy components when in the liquid state ($\Delta H_{ij}^{mix}$):

$$\Delta H_{mix} = \sum_{i=1;i\neq j}^{\frac{N(N-1)}{2}} \Omega_{ij} C_i C_j, \quad (1)$$

where $\Omega_{ij} = 4\Delta H_{ij}^{mix}$.

A negative mixing enthalpy favors homogeneous intermixing in a molten state and causes fast solidification kinetics. Conversely, a positive mixing enthalpy results in a poor intermixing and a formation of inhomogeneous material, with poor solidification kinetics. Hence, the mixing enthalpy can be utilized as a useful controlling parameter when designing the alloy's composition prior to its synthesis [27].

Another parameter influencing the phase stabilities in the HEAs is valence electron concentration (VEC). It is defined as a weighted average of the VECs ($v_i$) for the alloy components:

$$VEC = \sum_{i=1}^{N} (C_i v_i). \quad (4)$$

As we wrote in our review [16], most frequently, the reference values of $v_i$ when calculating VEC by Eq. (4) are taken as a total number of the electrons in the outer shell of the element [28] while more correct approach should account only electrons participating in the metallic bonding[1]. That is why, along with the conventionally calculated VEC (where the values of $v_i$ were taken from the number of electrons in the outer shell), we also used similarly calculated value (further denoted as VECP) where the reference values of $v_i$ corresponded to Pearson's valence of the $i$-th component [29].

The next key property considered in this work is the electronegativity mismatch ($\Delta\chi$) which can be calculated from the electronegativities of the alloy constituents according to the Eq. (5)):

$$\Delta\chi = \sqrt{\sum_{i=1}^{N} C_i \left(1 - \chi_i/\overline{\chi}\right)^2} \times 100\%, \quad (5)$$

where $\chi_i$ is electronegativity of the $i$-th component and $\overline{\chi} = \sum_{i=1}^{N} C_i\chi_i$ is the average electronegativity.

The last composition-dependent key property is the atomic size mismatch ($\delta$) related to the differences between the atomic radii of the alloy components:

$$\delta = \sqrt{\sum_{i=1}^{N} C_i \left(1 - r_i/\overline{r}\right)^2} \times 100\%, \quad (6)$$

where $r_i$ is atomic radius of the $i$-th component and $\overline{r} = \sum_{i=1}^{N} C_i r_i$ is the average atomic radius.

Other important factors usually not considered in the works describing key properties of the multicomponent alloys including HEAs but strongly affecting their hydrogen sorption properties include unit cell volume per one averaged metal atom ($V_M$) calculated from the crystallographic data, as well as the mixing enthalpy of the hydrogenated alloy ($\Delta H_{mix}^{H}$) calculated using Eq. (3) additionally accounting presence of hydrogen atoms (corresponding to the observed hydrogen-to-metal ratio, H/M) in the alloy's composition.

Detailed analysis of the key properties of HEAs described above is presented in our review [16] and references therein.

### *Background on Thermodynamics of Hydride–Forming HEAs*

The formation of hydrides of alloys is a complex thermodynamic phenomenon that relies primarily on factors such as the composition of the alloy, temperature, pressure, and the properties of the individual constituents. To elucidate the thermodynamic properties of the hydride formation, Gibbs free energy, enthalpy, entropy and temperature are the key parameters to consider.

Hydrogen storage utilizing any hydride-forming metal or alloy, $M$, involves direct (hydrogen uptake or hydrogenation) and reverse (hydrogen release or dehydrogenation) processes of the reversible reaction of the parent metal/alloy with hydrogen gas to form metal hydride ($MH_x$):

$$M + x/2\, H_2 \rightleftarrows MH_x. \quad (7)$$

The direction of Reaction (7) is determined by the sign of the change of the system Gibbs free energy ($\Delta G_H^\circ$) which depends on the process enthalpy ($\Delta H_H^\circ$), entropy ($\Delta S_H^\circ$) and temperature ($T$) [16][2]:

$$\Delta G_H^\circ = \Delta H_H^\circ - T\Delta S_H^\circ. \quad (8)$$

[1] The differences in $v_i$ taken from the various reference datasets are especially pronounced for the d-elements of Groups 7–12 [16].

[2] The superscript "°" refers to the standard conditions: $P$ = 1 atm = 0.101325 MPa; $T$ = 300 K.

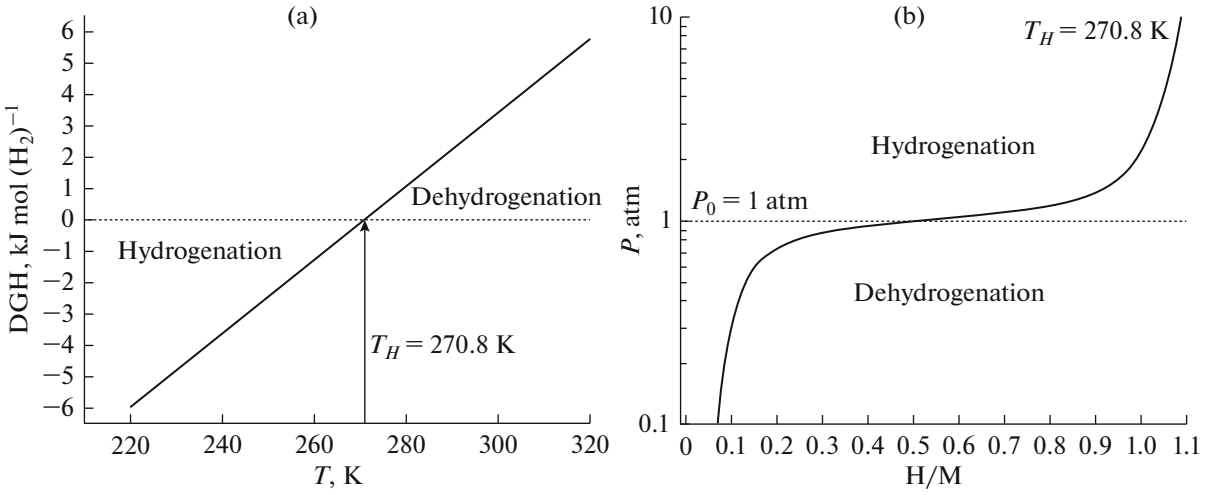


**Fig. 1.** Thermodynamic behavior of the system of $H_2$ gas with C14-$AB_2$-type HEA ($\Delta H_H^\circ = -31.88$ kJ mol $(H_2)^{-1}$; $\Delta S_H^\circ = -117.74$ J $K^{-1}$ mol $(H_2)^{-1}$) [32]. (a) Temperature dependence of the Gibbs free energy change. (b) Pressure–composition isotherm at $T_H = \Delta H_H^\circ/\Delta S_H^\circ$.

The value of $\Delta G_H^\circ$ also determines a relationship between the temperature and the equilibrium hydrogen pressure, $P_0 \approx$ const, in the plateau region of the $H_2$–M system (i.e., where the phases of α-solid solution of hydrogen in the host metal and β-hydride coexist), via the entropy and enthalpy changes for Reaction (7) through the van't Hoff equation [9]:

$$\mathrm{Ln}\left(P_0/P^\Theta\right) = \frac{\Delta G_H^\circ}{RT} = -\frac{\Delta S_H^\circ}{R} + \frac{\Delta H_H^\circ}{RT}, \qquad (9)$$

where $P^\Theta = 1$ atm $= 0.101325$ MPa is the reference pressure which corresponds to a standard state, $R$ is the universal gas constant, $T$ (K) is temperature, $\Delta S_H^\circ$ (J $K^{-1}$ mol $(H_2)^{-1}$) and $\Delta H_H^\circ$ (J mol $(H_2)^{-1}$) represent the standard entropy and enthalpy of hydrogenation, respectively.

For the spontaneous hydrogenation (direct process of Reaction (7)), the value of $\Delta G_H^\circ$ will be negative. Conversely, at $\Delta G_H^\circ > 0$, the reverse process (dehydrogenation) takes place spontaneously. When Reaction (7) is at equilibrium, $\Delta G_H^\circ$ is equal to zero that corresponds to the equilibrium temperature, $T = T_H$, which can be calculated as solution of Eq. (8) at $\Delta G_H^\circ = 0$:

$$T_H = \frac{\Delta H_H^\circ}{\Delta S_H^\circ}. \qquad (10)$$

The direct process of Reaction (7) is characterized by the negative entropy change ($\Delta S_H^\circ < 0$) because the condensed state is more ordered than the gaseous state due to the loss of at least one degree of translational freedom [30]. For most of hydride–forming alloys, $\Delta S_H^\circ$ is close to $-130$ J $K^{-1}$ mol $(H_2)^{-1}$ since the major contribution to the reaction entropy change is from the change in state from molecular hydrogen gas, $S^\Theta(H_2(g)) = 130.7$ J $K^{-1}$ $mol^{-1}$, to hydrogen in the solid for which the entropy, $S^\Theta(H(s))$, is assumed to be zero [31].

The change of direction of Reaction (7) from the direct (hydrogenation) to the reverse (dehydrogenation) will take place when the value of $\Delta G_H^\circ$ changes it sign from "–" to "+" passing zero. Taking into account that the second term of right-hand part of Eq. (8) will be always positive, it may happen only when $\Delta H_H^\circ < 0$, i.e., if the hydrogenation is exothermic. In doing so, at the pressure of 1 atm which corresponds to the standard state and $T < T_H$, spontaneous hydrogenation occurs while at $T > T_H$ it will be reversed to dehydrogenation passing equilibrium at $T = T_H$. Accordingly, at $T = T_H$ and $P > P_0$, $P = P_0$ and $P < P_0$, hydrogenation, equilibrium and dehydrogenation, respectively, will be observed. This is illustrated by Fig. 1 derived from our recently published experimental data [32] for the C14-$AB_2$-type high entropy alloy $Ti_{0.85}Zr_{0.15}Cr_{0.2}Mn_{1.22}Ni_{0.22}V_{0.3}Fe_{0.06}$ prepared by arc melting.

Though the described approach does not take into account such features of real hydrogen—metal systems like hysteresis and plateau slope [33], it is useful for deriving empiric interrelation between the key properties of the alloys analyzed in this study and thermody-

**Table 1.** Summary of the data on mixing entropies for the alloys analyzed in this work

| Structure | Number of entries | | | |
|---|---|---|---|---|
| | LEA: $\Delta S_{mix} \le R$ | MEA: $R < \Delta S_{mix} \le 1.5R$ | HEA: $\Delta S_{mix} > 1.5R$ | SUM |
| BCC | 6 | 59 | 36 | 101 |
| $AB_2$ | 29 | 97 | 63 | 189 |
| $AB_5$ | 2 | 56 | 6 | 64 |
| Total | *37* | *212* | *105* | *354* |

**Table 2.** List of the regression coefficients and the corresponding input variables

| Coefficient $A_i$ | Variable $X_i$ | Meaning (units) | Notation |
|---|---|---|---|
| $A_0$ | – | Free term at all $X_i = 0$ | – |
| $A_1$ | $X_1$ | Unit cell volume per one averaged metal atom, Å$^3$ | $V_M$ |
| $A_2$ | $X_2$ | Enthalpy of mixing for the alloy, kJ g-at(M)$^{-1}$ | $\Delta H_{mix}$ |
| $A_3$ | $X_3$ | Enthalpy of mixing for the hydride, kJ g-at(M + H)$^{-1}$ | $\Delta H^H_{mix}$ |
| $A_4$ | $X_4$ | Entropy of mixing for the alloy, J K$^{-1}$ g-at(M)$^{-1}$ | $\Delta S_{mix}$ |
| $A_5$ | $X_5$ | Electronegativity mismatch, % | $\Delta\chi$ |
| $A_6$ | $X_6$ | Size mismatch, % | $\delta$ |
| $A_7$ | $X_7$ | Valence electron concentration determined from total number of electrons in the outer shell (VEC) or Pearson's valence (VECP) | VEC or VECP |

namics of their interaction with $H_2$ gas with the help of machine learning.

## METHODOLOGY

### *Dataset*

The reference data for the BCC and $AB_2$-type Laves phase alloys was taken from our review articles [10, 16] and supplemented by the data for the $AB_5$-type intermetallics [34–47]. The database consists of a total of 354 entries, of which 101 are BCC, 64 are $AB_5$, and 189 are $AB_2$–based Laves phase (156 C14 and 33 C15) alloys. Each entry contains information about VEC, VECP, $\delta$, $\Delta\chi$, $\Delta H_{mix}$, and $\Delta S_{mix}$ for every alloy (calculated from its composition). Additionally, the values of $V_M$ were included, along with the hydrogen storage properties, i.e., H/M ratio, as well as standard enthalpy ($\Delta H^\circ_H$) and entropy ($\Delta S^\circ_H$) of the hydrogenation. The standard Gibbs free energy of hydrogen absorption ($\Delta G^\circ_H$), and temperature ($T_H$) at which $\Delta G^\circ_H = 0$) were calculated for each material from the values of $\Delta H^\circ_H$ and $\Delta S^\circ_H$, using Eqs. (8) and (10).

Table 1 summarizes the data about mixing entropies for the alloys analyzed in this work. The inclusion of low- (LEA) and medium-entropy alloys (MEA) along with the high-entropy (HEA) ones is to allow the model developed in this work to predict all the three categories.

### *Linear Regression*

The correlations between the input variables ($X_i$) and the response values ($Y$) were analyzed using the simplest linear regression equation:

$$Y = A_0 + \sum_{i=1}^{7} A_i X_i, \quad (11)$$

where $Y = H/M$, $\Delta G^\circ_H$ or $T_H$, and the regression coefficients $A_1 ... A_7$ determine the forecasted effects of the corresponding key properties accounted by the variables $X_1 ... X_7$ on the response value.

The list of the regression coefficients and the corresponding input variables is presented in Table 2.

The values of the regression coefficients $A_0 ... A_7$ were calculated by the fitting of the reference dataset, separately for the BCC, C14-$AB_2$, C15-$AB_2$ and $AB_5$ alloys. Separate fitting sessions were also applied for the different response values (H/M, $\Delta G^\circ_H$ or $T_H$), as well as for the valence electron concentrations taken

from the different starting data (VEC or VECP). In total, 24 fitting sessions (4 for different alloy structures × 3 for different response values × 2 for different reference data for valence electron concentrations) were done.

For the evaluation of adequacy of the fitting results, the reference ($x = Y_k$) and calculated ($y = Y(x_k)$) values of the responses were plotted together and fitted using linear regression equation:

$$y = a_0 + a_1 x. \quad (12)$$

Furthermore, the following adequacy parameters have been determined:

- Total sum of squares (*TSS*):

$$TSS = \sum_{k=1}^{N} y_k^2; \quad (13)$$

- Residual sum of squares (*RSS*):

$$RSS = \sum_{k=1}^{N} [y_k - (a_0 + a_1 x_k)]^2; \quad (14)$$

- Coefficient of determination ($R^2$):

$$R^2 = 1 - \frac{RSS}{TSS}; \quad (15)$$

- Mean square error (*MSE*):

$$MSE = \frac{RSS}{N - 2}. \quad (16)$$

### *Sensitivity Analysis*

Application of the simplest linear regression model (Eq. (11)) is useful for the estimation of the effect of the parameter change on the changes of the response parameter (sensitivity). It is proportional to the value of $A_i$ ($i \geq 1$). For the correct comparison when the scales of parameters $X_i$ are different, it is necessary to introduce normalization coefficient assumed to be related to the range of the parameter change.

Sensitivity of a function $Y(X_1, X_2, \ldots X_n)$ to the argument $X_i$ can be estimated from its partial derivative, $\partial Y/(\partial X_i)$ . For the uniform scaling of the argument $X_i$, it can be transformed to a normalized argument, $t_i$, as:

$$t_i = \frac{X_i - X_i^{MIN}}{X_i^{MAX} - X_i^{MIN}}, \quad (17)$$

where $X_i^{MIN}$ and $X_i^{MAX}$ are the minimum and maximum values of the argument $X_i$; so, the variation of each $X_i$ between $X_i^{MIN}$ and $X_i^{MAX}$ will result in the uniform variation of $t_i$ between 0 and 1. Accordingly:

$$\frac{\partial Y}{\partial X_i} = \frac{\partial Y}{\partial t_i}\frac{\partial t_i}{\partial X_i} = \frac{\partial Y}{\partial t_i}\frac{1}{X_i^{MAX} - X_i^{MIN}}, \quad (18)$$

or, taking into account Eq. (11):

$$\frac{\partial Y}{\partial t_i} = \frac{\partial Y}{\partial X_i}\left(X_i^{MAX} - X_i^{MIN}\right) = A_i\left(X_i^{MAX} - X_i^{MIN}\right) = A_i \Delta X_i, \quad (19)$$

where $\Delta X_i = X_i^{MAX} - X_i^{MIN}$ is the variation range of the $i$-th input variable.

Finally, the sensitivity to the argument $X_i$ ($s_i$) will be equal to:

$$s_i = \frac{A_i}{\Delta X_i}. \quad (20)$$

### *Validation and Experimental Procedure*

For the validation of the regression analysis results, we used the recently published reference data on the BCC [48], C14-$AB_2$ [49], C15-$AB_2$ [50] and $AB_5$ [51] alloys. Additionally, we have experimentally tested several hydrogen storage alloys of BCC, C14-$AB_2$ and $AB_5$ types. The combined data on the alloys' structure, composition and hydrogen sorption properties are summarized in Table 3.

The alloys for the experimental tests were prepared from industrial-grade quality metals (purity 99.8%) using small-to-medium scale (single batch up to 1 kg) arc-melting facility (non-consumable tungsten electrode and water-cooled hearth) under atmosphere of the purified argon. To provide compositional homogeneity, each ingot was turned over and re-melted three times. The alloys were studied in the as-cast state.

The elemental composition of the alloys was studied by the atomic emission spectroscopy with inductively coupled plasma (iCAP 6300 Thermo Electron instrument) and X-ray fluorescent analysis (Rigaku Nex DE VS instrument). The input parameters for the regression analysis were calculated from the alloys composition according to the results of analysis.

The X-ray diffraction analysis (XRD, Rigaku MiniFlex instrument) has confirmed the phase composition of the alloys when the content of the major phase (BCC, C14-$AB_2$ or $AB_5$) exceeded 95%. The lattice periods of the major phase were further calculated from the XRD data followed by the calculation of the unit cell volume starting from the lattice periods, unit cell geometry and number of the formula units in the unit cell.

Hydrogen sorption properties of the alloys were studied using H-Sorb 2600 PCT gas sorption analyzer (Beijing CI Ultrametrics Technology Co, Ltd) by measuring hydrogen absorption and desorption pressure–composition isotherms ($T$ = 293–353 K, $P(H_2)$ = 0.01–5.0 MPa). The value of H/M (sixth column of Table 3) used for the comparison with the regression analysis results was directly measured as a maximum hydrogen absorption capacity of the alloy at the minimum temperature and the maximum hydro-

**Table 3.** Hydrogen sorption properties of the samples taken for the model validation

| Structure | | | Composition | Reference | Hydrogen sorption properties | | |
|---|---|---|---|---|---|---|---|
| type | lattice periods, Å | unit cell volume per metal atom ($V_M$, Å$^3$) | | | H/M | $\Delta S_H^\circ$, J K$^{-1}$ mol $(H_2)^{-1}$ | $\Delta H_H^\circ$, J mol $(H_2)^{-1}$ |
| BCC | $a = 3.035$ | 13.98 | $V_{75.02}Ti_{9.97}Zr_{7.48}Cr_{7.52}$ | This work | 1.80 | −132.28 | −43.32 |
| | $a = 3.040$ | 14.05 | $V_{35}Ti_{35}Cr_{10}Fe_{10}Ni_{10}$ | [48] | 1.18 | −130.99 | −47.83 |
| C14-$AB_2$ | $a = 4.891$<br>$c = 8.006$ | 13.82 | $Ti_{0.87}Zr_{0.13}Cr_{0.22}Mn_{1.32}Ni_{0.14}V_{0.31}Fe_{0.06}$ | This work | 0.92 | −117.74 | −31.88 |
| | $a = 4.949$<br>$c = 8.119$ | 14.35 | $Ti_{0.5}Zr_{0.5}Mn_{0.62}Fe_{0.67}Cr_{0.67}$ | This work | 0.99 | −115.15 | −30.77 |
| | $a = 4.999$<br>$c = 8.148$ | 14.69 | TiZrFeMnCrV | [49] | 1.16 | −117.86 | −44.07 |
| C15-$AB_2$ | $a = 7.034$ | 14.50 | $Ti_{0.15}Zr_{0.85}La_{0.03}Ni_{1.126}Mn_{0.657}V_{0.113}Fe_{0.113}$ | [50] | 1.10 | −113.33 | −35.25 |
| $AB_5$ | $a = 4.979$<br>$c = 4.056$ | 14.52 | $La_{0.41}Ce_{0.59}Ni_{3.5}Co_{0.53}Mn_{0.57}Al_{0.22}Cr_{0.08}$ | This work | 0.92 | −112.20 | −35.61 |
| | $a = 5.022$<br>$c = 4.034$ | 14.68 | $La_{0.65}Ce_{0.2}Ca_{0.15}Ni_{4.5}Mn_{0.4}Al_{0.1}$ | [51] | 1.11 | −107.56 | −35.31 |

gen pressure. The values of $\Delta G_H^\circ$ (at $T = 300$ K) and $T_H$ were calculated using equations (8) and (10), respectively, from the values of $\Delta S_H^\circ$ and $\Delta H_H^\circ$ (two last columns of Table 3) calculated by the fitting of the experimental isotherms with the model [33].

## RESULTS AND DISCUSSION

### *Statistics of the Reference Data*

Figure 2 shows distribution histograms of the mixing entropies (A), hydrogen storage capacities in H/M units (B), equilibrium temperatures (C) and standard Gibbs free energies of hydrogenation (D) for the single-phase alloys of different types analyzed in this work.

As it can be seen from Fig. 2a and Table 1, most of the studied alloys represent the medium-temperature ones (MEAs). This is caused by specifics of the multicomponent hydrogen storage alloys (especially, intermetallic ones) which must have a certain balance of the components characterized by high (e.g., Ti, Zr, V) and low (e.g., Ni, Cr, Mn, Fe) affinity to hydrogen and must not always present in the alloy's composition in the equal atomic fractions [6, 16].

For the hydrogen absorption capacities of the alloys, the distribution maxima correspond to the typical values for the similar low- and medium-entropy hydride-forming alloys: 1.9–2.0 H/M for BCC and 0.8–1.0 H/M for the $AB_2$- and $AB_5$-type intermetallics (Fig. 2b). Similar situation is observed for the equilibrium temperatures (Fig. 2c; $T_H$ = 220–240 K for $AB_2$, 300–320 K for BCC and 380–400 K for $AB_5$) and, finally, for $\Delta G_H^\circ$ (Fig. 2d; from −6.6 to −5.0 kJ mol $(H_2)^{-1}$ for $AB_5$, from −5.1 to −3.2 kJ mol $(H_2)^{-1}$ for BCC and from +6.6 to +8.3 kJ mol $(H_2)^{-1}$ for $AB_2$). These observations additionally confirm our statement that hydrogen sorption performances of LEAs, MEAs and HEAs are very similar and primarily depend on the structural features and the nature of their constituents rather than on other key properties of the alloys which ignore these features [16].

### *Linear Regression Analysis*

Table 4 presents the results of regression analysis (Eq. (11)) of the reference data for the alloys analyzed in this work when the fitting parameters $A_0 ... A_7$ were calculated by the separate fitting of each response (H/M, $T_H$ and $\Delta G_H^\circ$) for the datasets representing the single-phase alloys with BCC, C14-$AB_2$, C15-$AB_2$ and $AB_5$ structures when the reference data on the valence electron concentration were taken either from the total number of electrons in outer shells of the constituent elements (VEC), or from their Pearson's valence (VECP).

It is seen that the simple linear regression (Eq. (11)) gives acceptable adequacy of the calculated and reference data, with the values of correlation coefficient, $R^2$, above 0.5 and mostly above 0.8–0.9.

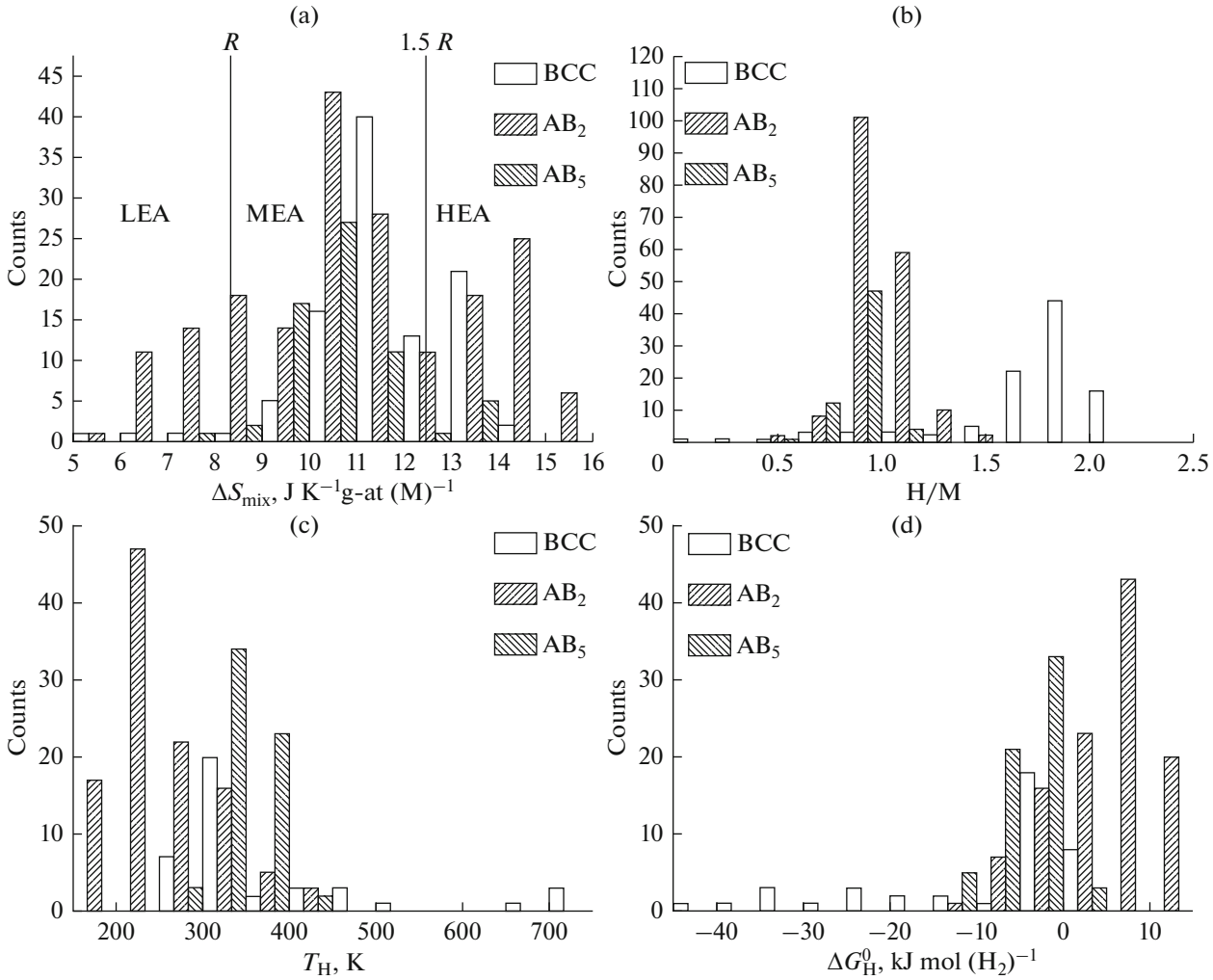


**Fig. 2.** Distribution histograms of mixing entropies (a), hydrogen sorption capacities (b), standard Gibbs free energies of hydrogen absorption (c) and equilibrium temperatures (d) for the alloys analyzed in this work.

The poorer correlations for $T_H$, $\Delta G_H^\circ$ ($AB_5$), H/M (BCC), have their origin in the fact that noticeable deviations of these parameters from the trend line result in the appearance of the non-zero calculated intercept ($a_0 > 0$ in Eq. (12)) that, in turn, causes the decrease of the calculated slope ($0 < a_1 < 1$ in Eq. (12)) proportional to $R^2$. When comparing the reference and calculated data using Eq. (12) and fixing the intercept $a_0 = 0$ (that should be in the case of complete adequacy), the values of $R^2$ for all the datasets were above 0.9.

Comparison of the calculated and reference data for the alloys of different structures taken together (Eq. (12) without fixing the intercept $a_0$; see Table 5 and Fig. 3) yields good adequacy parameters, with the values of $R^2$ above 0.9 for all the response values.

It is also seen from Table 4 that the fitting results obtained for the different reference data taken for the valence electron concentration are quite close to each other.

### *Sensitivity Analysis*

Table 6 presents the values of sensitivities of the response parameters (Eq. (11)) to the changes of input variables $X_1 \ldots X_7$ normalized using Eq. (17). The sensitivities were calculated from the fitted values of the regression coefficients $A_1 \ldots A_7$ using Eq. (20). The results of the sensitivity analysis are presented as graphs (Fig. 4) plotted for the reference data on valence electron concentration taken from the Pearson's valence.

The calculated values of the sensitivities taken for the different response parameters (H/M, $\Delta G_H^\circ$ and $T_H$) correlate with each other when the sensitivities for both H/M and $T_H$ exhibit proportionality to the corre-

**Table 4.** Summary of separate fitting sessions of the reference data with Eq. (11)

| Structure | $Y$ | $N$ | VEC data | Variation range of the input variable | | | | | | | Regression coefficients | | | | | | | | $R^2$ |
|---|---|---|---|---|---|---|---|---|---|---|---|---|---|---|---|---|---|---|---|
| | | | | $\Delta X_1$ | $\Delta X_2$ | $\Delta X_3$ | $\Delta X_4$ | $\Delta X_5$ | $\Delta X_6$ | $\Delta X_7$ | $A_0$ | $A_1$ | $A_2$ | $A_3$ | $A_4$ | $A_5$ | $A_6$ | $A_7$ | |
| BCC | H/M | 100 | VEC | 7.32 | 21.75 | 23.86 | 9.13 | 17.27 | 6.83 | 2.55 | −0.98 | −0.01 | 0.00 | −0.10 | 0.00 | −0.03 | −0.01 | 0.23 | 0.77 |
| | | | VECP | 7.32 | 21.75 | 23.86 | 9.13 | 17.27 | 6.83 | 2.45 | −0.36 | −0.01 | −0.01 | −0.09 | 0.00 | −0.03 | −0.01 | 0.14 | 0.76 |
| | $T_H$ | 39 | VEC | 5.60 | 15.86 | 7.78 | 8.09 | 10.80 | 5.55 | 1.51 | −2198.34 | 79.06 | −5.90 | −31.22 | −4.71 | −8.08 | 37.53 | 128.52 | 0.91 |
| | | | VECP | 5.60 | 15.86 | 7.78 | 8.09 | 10.80 | 5.55 | 0.90 | −2989.48 | 71.93 | −9.29 | −45.14 | 2.93 | −5.36 | 35.45 | 241.91 | 0.92 |
| | $\Delta G^\circ_H$ | | VEC | 5.60 | 15.86 | 7.78 | 8.09 | 10.80 | 5.55 | 1.51 | 261.78 | −8.15 | 0.31 | 3.62 | 1.97 | 1.23 | −2.85 | −17.85 | 0.93 |
| | | | VECP | 5.60 | 15.86 | 7.78 | 8.09 | 10.80 | 5.55 | 0.90 | 328.65 | −6.98 | 0.76 | 4.99 | 0.94 | 0.80 | −2.40 | −27.75 | 0.93 |
| C14-$AB_2$ | H/M | 117 | VEC | 3.06 | 26.45 | 9.29 | 8.21 | 10.64 | 5.03 | 2.02 | −0.69 | 0.01 | 0.01 | −0.07 | 0.01 | 0.01 | 0.00 | 0.06 | 0.76 |
| | | | VECP | 3.06 | 26.45 | 9.29 | 8.21 | 10.64 | 5.03 | 1.00 | −1.46 | 0.02 | 0.00 | −0.07 | 0.01 | 0.01 | −0.01 | 0.17 | 0.77 |
| | $T_H$ | 77 | VEC | 2.07 | 26.45 | 7.46 | 6.46 | 10.11 | 4.33 | 1.26 | −753.39 | 63.62 | −3.28 | 2.81 | 8.02 | −19.05 | 46.45 | −37.43 | 0.86 |
| | | | VECP | 2.07 | 26.45 | 7.46 | 6.46 | 10.11 | 4.33 | 0.40 | −513.56 | 62.15 | −1.79 | 2.34 | 7.59 | −19.91 | 46.58 | −79.86 | 0.86 |
| | $\Delta G^\circ_H$ | | VEC | 2.07 | 26.45 | 7.46 | 6.46 | 10.11 | 4.33 | 1.26 | 121.97 | −7.31 | 0.35 | −0.22 | −0.84 | 2.07 | −4.62 | 3.23 | 0.86 |
| | | | VECP | 2.07 | 26.45 | 7.46 | 6.46 | 10.11 | 4.33 | 0.40 | 97.43 | −7.09 | 0.22 | −0.18 | −0.79 | 2.14 | −4.64 | 7.37 | 0.86 |
| C15-$AB_2$ | H/M | 33 | VEC | 0.89 | 20.54 | 7.21 | 6.53 | 4.40 | 5.56 | 2.03 | −3.43 | 0.24 | −0.05 | −0.12 | −0.05 | −0.25 | 0.28 | −0.19 | 0.93 |
| | | | VECP | 0.89 | 20.54 | 7.21 | 6.53 | 4.40 | 5.56 | 0.99 | 11.31 | −0.51 | 0.00 | −0.12 | −0.03 | −0.01 | 0.11 | −1.05 | 0.95 |
| | $T_H$ | 24 | VEC | 0.89 | 20.54 | 7.21 | 6.53 | 4.40 | 5.56 | 2.03 | −2442.12 | 150.50 | −0.33 | −1.73 | 23.25 | −39.67 | 17.65 | 88.92 | 0.96 |
| | | | VECP | 0.89 | 20.54 | 7.21 | 6.53 | 4.40 | 5.56 | 0.99 | −859.92 | 44.56 | −0.31 | −2.50 | 21.61 | −23.05 | 28.76 | 39.05 | 0.96 |
| | $\Delta G^\circ_H$ | | VEC | 0.89 | 20.54 | 7.21 | 6.53 | 4.40 | 5.56 | 2.03 | 237.24 | −12.79 | −0.38 | 0.00 | −3.17 | −0.15 | 1.16 | −5.21 | 0.96 |
| | | | VECP | 0.89 | 20.54 | 7.21 | 6.53 | 4.40 | 5.56 | 0.99 | 158.76 | −7.34 | −0.34 | 0.04 | −3.06 | −0.90 | 0.39 | −3.05 | 0.96 |
| $AB_5$ | H/M | 59 | VEC | 0.96 | 7.31 | 4.61 | 6.13 | 1.48 | 1.98 | 1.15 | −1.37 | 0.09 | 0.00 | −0.12 | 0.00 | −0.04 | 0.01 | 0.01 | 0.95 |
| | | | VECP | 0.96 | 7.31 | 4.61 | 6.13 | 1.48 | 1.98 | 0.64 | −0.20 | 0.04 | 0.00 | −0.12 | 0.00 | −0.05 | 0.01 | −0.06 | 0.95 |
| | $T_H$ | 57 | VEC | 0.96 | 7.31 | 4.61 | 6.13 | 1.48 | 1.98 | 1.15 | −2321.65 | 107.53 | −12.72 | −15.49 | 11.13 | −9.28 | 6.52 | 80.54 | 0.59 |
| | | | VECP | 0.96 | 7.31 | 4.61 | 6.13 | 1.48 | 1.98 | 0.64 | −162.01 | 38.72 | −10.25 | −16.56 | 1.23 | −9.84 | 12.91 | −84.91 | 0.64 |
| | $\Delta G^o_H$ | | VEC | 0.96 | 7.31 | 4.61 | 6.13 | 1.48 | 1.98 | 1.15 | 289.46 | −11.64 | 1.15 | 1.33 | −1.30 | 0.52 | −0.40 | −9.72 | 0.56 |
| | | | VECP | 0.96 | 7.31 | 4.61 | 6.13 | 1.48 | 1.98 | 0.64 | 18.70 | −2.93 | 0.84 | 1.48 | −0.14 | 0.67 | −1.16 | 10.79 | 0.65 |

**Table 5.** Adequacy parameters of the linear regression modelling (Eq. (11)) when comparing the reference data and calculation results for the alloys belonging to all studied classes for VEC calculated from the Pearson's valence

| Response | Linear regression coefficients: $y = a_0 + a_1x$ | | Statistics | | | | |
|---|---|---|---|---|---|---|---|
| | $a_0$ | $a_1$ | $N$ | $TSS$ | $RSS$ | $R^2$ | $MSE$ |
| H/M | 0.09 ± 0.02 | 0.92 ± 0.02 | 309 | 54.322 | 4.1237 | 0.9241 | 0.01343 |
| $T_H$ | 19 ± 6 | 0.94 ± 0.02 | 197 | 1463463 | 92103 | 0.9371 | 472.33 |
| $\Delta G_H^\circ$ | –0.04 ± 0.15 | 0.94 ± 0.02 | 197 | 16002 | 874 | 0.9454 | 4.4813 |

sponding negated sensitivities for $\Delta G_H^\circ$. Taking into account close values of the hydrogenation standard entropies, $\Delta S_H^\circ$, for the metallic hydrides (see section "Background on thermodynamics of hydride–forming HEAs" above), the standard Gibbs free energy of the hydrogenation determines stability of hydrides proportional to the negated standard enthalpy of the hydrogenation, $-\Delta H_H^\circ$. Accordingly, the more negative the value of $\Delta G_H^\circ$, will be, the higher will be both hydrogen-to-metal ratio and the equilibrium temperature.

It should be also noted that correlations between the sensitivities of $\Delta G_H^\circ$ and H/M are poorer, and the

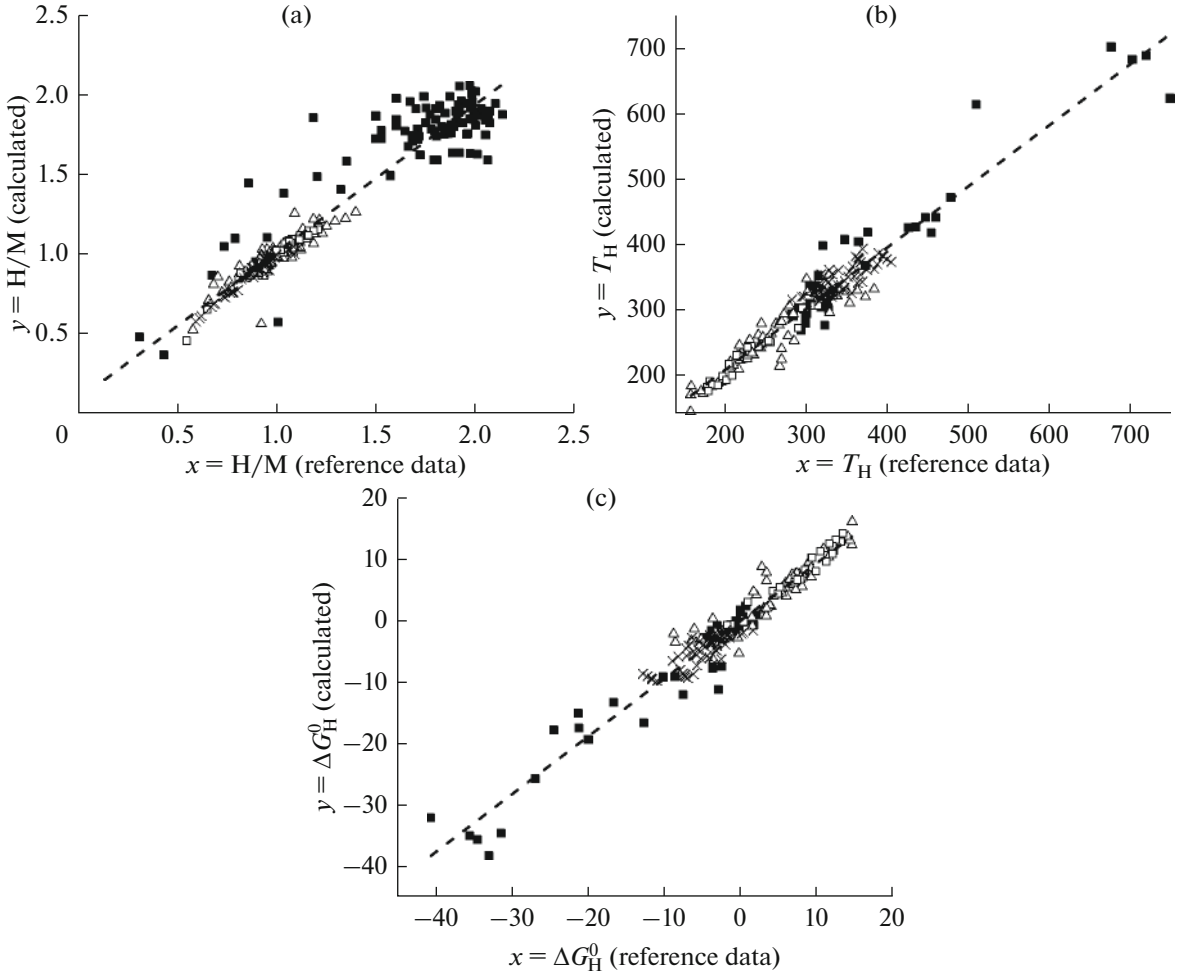


**Fig. 3.** Comparison of the regression analysis (Eq. (11)) results ($y$) for H/M (A), $T_H$ (B) and $\Delta G_H^\circ$ (C) response values with the reference data ($x$) for the alloys studied in this work (■—BCC; △—C14-$AB_2$; □—C15-$AB_2$; ×—$AB_5$; dashed line—common linear fit $y = a_0 + a_1x$, see Table 5). The graphs are presented for VEC calculated from the Pearson's valence.

**Table 6.** Summary of sensitivities of the response parameters (Eq. (11)) to the normalized input variables for the single-phase alloys analyzed in this work. The units of sensitivities correspond to the units of the response parameters (dimensionless for H/M, kJ mol$(H_2)^{-1}$ for $\Delta G^o_H$, K for $T_H$)

| Dataset | | | Sensitivity for the variable | | | | | | |
|---|---|---|---|---|---|---|---|---|---|
| Structure | Response | VEC data | $X_1$ ($V_M$) | $X_2$ ($\Delta H_{mix}$) | $X_3$ ($\Delta H^H_{mix}$) | $X_4$ ($\Delta S_{mix}$) | $X_5$ ($\Delta\chi$) | $X_6$ ($\delta$) | $X_7$ (VEC) |
| BCC | H/M | VEC | 0.0018 | 0.0001 | −0.0033 | 0.0014 | −0.0012 | −0.0034 | 0.0137 |
| | | VECP | 0.0032 | 0.0001 | −0.0030 | 0.0013 | −0.0012 | −0.0017 | 0.0201 |
| | $T_H$ | VEC | 18.8391 | 0.1495 | 0.0718 | 0.5168 | −0.2970 | 5.4832 | 10.4678 |
| | | VECP | 18.1452 | 0.1937 | 0.0647 | 0.3896 | −0.1886 | 5.1085 | 12.1338 |
| | $\Delta G^\circ_H$ | VEC | −1.8132 | 0.0096 | 0.0329 | −0.1185 | 0.0473 | −0.3529 | −1.7480 |
| | | VECP | −1.6926 | 0.0021 | 0.0339 | −0.0970 | 0.0291 | −0.2891 | −1.9976 |
| C14-$AB_2$ | H/M | VEC | 0.0033 | −0.0001 | −0.0027 | −0.0006 | 0.0008 | −0.0002 | 0.0071 |
| | | VECP | 0.0071 | −0.0001 | −0.0027 | −0.0007 | 0.0009 | −0.0003 | 0.0205 |
| | $T_H$ | VEC | 30.4269 | 0.0766 | 0.1376 | −0.5812 | −2.6277 | 2.4362 | −5.2103 |
| | | VECP | 26.9385 | 0.0528 | 0.1268 | −0.4877 | −2.7394 | 2.4722 | −15.2360 |
| | $\Delta G^\circ_H$ | VEC | −3.4919 | −0.0083 | −0.0122 | 0.0595 | 0.2862 | −0.2412 | 0.4283 |
| | | VECP | −3.0711 | −0.0064 | −0.0115 | 0.0496 | 0.2950 | −0.2463 | 1.4616 |
| C15-$AB_2$ | H/M | VEC | 0.2656 | 0.0010 | −0.0058 | 0.0094 | −0.0344 | 0.0181 | −0.0296 |
| | | VECP | −0.5689 | −0.0001 | −0.0061 | 0.0052 | −0.0016 | 0.0070 | −0.1612 |
| | $T_H$ | VEC | 169.0635 | 0.0069 | −0.0843 | −4.1236 | −5.5020 | 1.1212 | 13.6155 |
| | | VECP | 50.0603 | 0.0065 | −0.1219 | −3.8327 | −3.1970 | 1.8273 | 5.9790 |
| | $\Delta G^\circ_H$ | VEC | −14.3640 | 0.0081 | 0.0002 | 0.5626 | −0.0203 | 0.0738 | −0.7973 |
| | | VECP | −8.2441 | 0.0072 | 0.0022 | 0.5424 | −0.1253 | 0.0248 | −0.4676 |
| $AB_5$ | H/M | VEC | −0.0816 | −0.0004 | −0.0083 | −0.0029 | −0.0112 | 0.0055 | 0.0055 |
| | | VECP | −0.1269 | −0.0004 | −0.0083 | −0.0023 | −0.0119 | 0.0058 | −0.0083 |
| | $T_H$ | VEC | 81.5240 | 0.2821 | −0.6870 | −2.7977 | −1.5388 | 1.1204 | 12.5753 |
| | | VECP | 16.5611 | 0.2092 | −0.7217 | −0.2244 | −1.1690 | 1.5027 | −12.3516 |
| | $\Delta G^\circ_H$ | VEC | −9.5113 | −0.0259 | 0.0603 | 0.3401 | 0.1110 | −0.0864 | −1.5723 |
| | | VECP | −0.8998 | −0.0166 | 0.0649 | 0.0301 | 0.0820 | −0.1352 | 1.6332 |

absolute values of the sensitivities of H/M for the BCC alloys are much lower than the ones for other alloys. First of all, it is caused by the variation of the hydrogenation conditions at which the hydrogen capacities were reported.

Generally, the observed tendencies are similar to those identified for hydrogen sorption capacities of BCC and $AB_2$ HEAs [16] when the strongest effects were observed for unit cell volume ($X_1 = V_M$) and valence electron concentration ($X_7$ = VEC or VECP). The former parameter exhibits high negative values of the sensitivity ($s_1 < 0$) for $\Delta G^\circ_H$ that corresponds to the strong increase of the negated standard Gibbs energy and, accordingly, decrease of the plateau pressures (Eq. (9)) when increasing the unit cell volume. It is in line with well-known fact that the logarithm of the plateau pressure linearly decreases with the increase of the unit cell volume of the parent intermetallic [52].

Valence electron concentration exhibits less strong but still significant effect on the hydrogen sorption properties of the studied alloys. This effect is different for the different alloy structures and, for $AB_5$-type alloys, for the different datasets taken for VEC calculations (see last three rows in Table 6)[3]. If considering VECP, its effect ($s_7$) increases in the series BCC < C15-$AB_2$ < 0 < C14-$AB_2$ ≈ $AB_5$.

[3] Most probably, the origin of this deviation is in significant difference of the reference data for Ni (outer shell VEC = 10, Pearson's maximum valence VECP = 6 [16]) to be main component in most of $AB_5$-type hydrogen storage alloys.

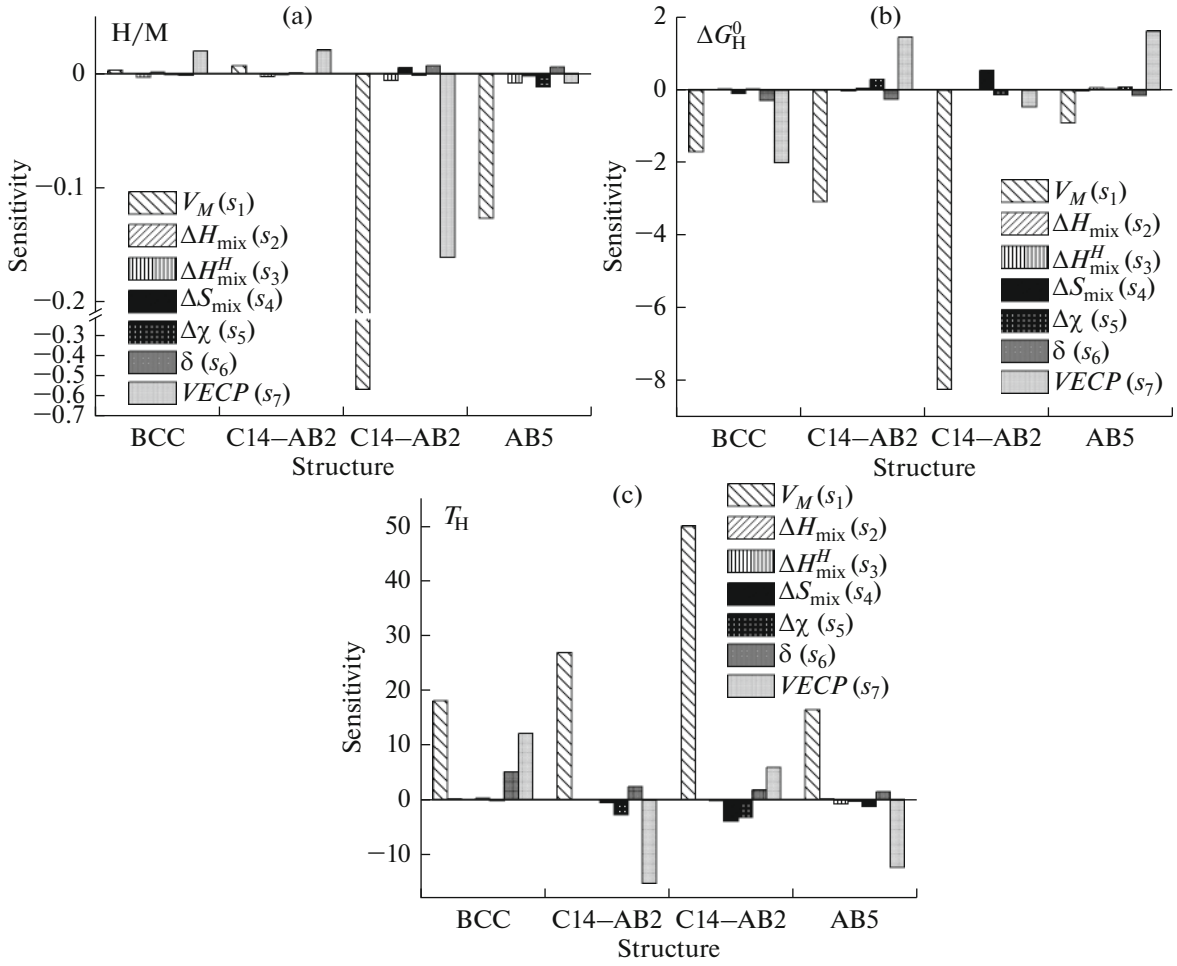


**Fig. 4.** Sensitivities of the response parameters (Eq. (11)) to the normalized input variables for the single-phase alloys analyzed in this work when VEC data were taken from Pearson's valence.

The strong effect of valence electron concentration on the hydrogen sorption properties of the high entropy alloys was reported earlier [16, 53].

A certain effect was also observed for the electronegativity mismatch ($X_5 = \Delta\chi$) while the sensitivities to other input variables were found to be much lower on their absolute values than the ones for $X_1 = V_M$, $X_7$ = VECP and $X_5 = \Delta\chi$. An exception is the mixing entropy ($X_4 = \Delta S_{mix}$) for C15-$AB_2$ intermetallics whose effect, $s_4 < 0$ for $\Delta G^\circ_H$ is comparable with the effect of the electronegativity mismatch ($s_5 < 0$). However, considering relatively small number of the processed entries for this class of the alloys (see the third column of Table 4), this finding needs additional verification.

The results of the sensitivity analysis are in a satisfactory correspondence with the conclusions of Ek et al. [54] who evaluated compositional effects on hydrogen sorption performances of 15 Ti–V–Zr–Nb–Hf-based HEAs with BCC structure and found linear dependencies of H/M or onset temperature of hydrogen desorption on the volumetric expansion of the crystal lattice per metal atom, valence electron concentration, and average electronegativity of the alloys while no correlation was observed for the size mismatch.

### *Validation*

The experimental and reference data on the hydrogen sorption properties of the alloys selected for the validation of the regression analysis modelling (Table 3) have been compared with the calculation results using Eq. (11) and the input variables presented separately ($V_M$) or calculated from the composition of the pristine ($\Delta H_{mix}$, $\Delta S_{mix}$, $\Delta\chi$, $\delta$, VECP) or hydrogenated ($\Delta H^H_{mix}$) alloy.

It is seen from Table 7 that the realistic predictions of the linear regression modelling were achieved for the equilibrium temperatures, $T_H$, when the deviations, (Calculated–Observed), were between –55 and

**Table 7.** Comparison of the observed hydrogen sorption characteristics with the ones calculated using results of the linear regression analysis (Eq. (11), Table 4) for VEC calculated from the Pearson's valence

| Structure | Alloy | Reference | Response ($Y$) | Observed | Calculated | Deviation |
|---|---|---|---|---|---|---|
| BCC | $V_{75.02}Ti_{9.97}Zr_{7.48}Cr_{7.52}$ | This work | H/M | 1.80 | 1.85 | +0.05 |
| | | | $T_H$ (K) | 327 | 303 | −24 |
| | | | $\Delta G_H^\circ$ kJ mol $(H_2)^{-1}$ | −3.636 | −7.739 | −4.103 |
| | $V_{35}Ti_{35}Cr_{10}Fe_{10}Ni_{10}$ | [48] | H/M | 1.18 | 1.86 | +0.68 |
| | | | $T_H$ (K) | 365 | 403 | +38 |
| | | | $\Delta G_H^\circ$ kJ mol $(H_2)^{-1}$ | −8.533 | −9.025 | −0.492 |
| C14-$AB_2$ | $Ti_{0.5}Zr_{0.5}Mn_{0.62}Fe_{0.67}Cr_{0.67}$ | This work | H/M | 0.99 | 1.00 | +0.01 |
| | | | $T_H$ (K) | 271 | 281 | +10 |
| | | | $\Delta G_H^\circ$ kJ mol $(H_2)^{-1}$ | 3.442 | 2.035 | −1.407 |
| | $Ti_{0.87}Zr_{0.13}$ $Cr_{0.22}Mn_{1.32}Ni_{0.14}V_{0.31}Fe_{0.06}$ | This work | H/M | 0.92 | 0.56 | −0.36 |
| | | | $T_H$ (K) | 271 | 240 | −31 |
| | | | $\Delta G_H^\circ$ kJ mol $(H_2)^{-1}$ | 3.442 | 6.511 | +3.069 |
| | TiZrFeMnCrV | [49] | H/M | 1.16 | 1.11 | −0.05 |
| | | | $T_H$ (K) | 374 | 319 | −55 |
| | | | $\Delta G_H^\circ$ kJ mol $(H_2)^{-1}$ | −8.712 | −2.106 | +6.606 |
| C15-$AB_2$ | $Ti_{0.15}Zr_{0.85}La_{0.03}$ $Ni_{1.126}Mn_{0.657}V_{0.113}Fe_{0.113}$ | [50] | H/M | 1.10 | 1.09 | −0.01 |
| | | | $T_H$ (K) | 311 | 306 | −5 |
| | | | $\Delta G_H^\circ$ kJ mol $(H_2)^{-1}$ | −1.251 | −0.614 | +0.637 |
| $AB_5$ | $La_{0.41}Ce_{0.59}$ $Ni_{3.5}Co_{0.53}Mn_{0.57}Al_{0.22}Cr_{0.08}$ | This work | H/M | 0.92 | 0.90 | −0.02 |
| | | | $T_H$ (K) | 317 | 339 | +21 |
| | | | $\Delta G_H^\circ$ kJ mol $(H_2)^{-1}$ | −1.950 | −3.823 | −1.873 |
| | $La_{0.65}Ce_{0.2}Ca_{0.15}$ $Ni_{4.5}Mn_{0.4}Al_{0.1}$ | [51] | H/M | 1.11 | 1.05 | −0.07 |
| | | | $T_H$ (K) | 328 | 341 | +13 |
| | | | $\Delta G_H^\circ$ kJ mol $(H_2)^{-1}$ | −3.043 | −4.089 | −1.046 |

+38 K, or mostly below ±(10–15)% of the observed/reference value.

For the hydrogen sorption capacities, as a rule, the deviations did not exceed ±0.1 H/M, but for the BCC alloy $V_{35}Ti_{35}Cr_{10}Fe_{10}Ni_{10}$ and C14 Laves phase $Ti_{0.87}Zr_{0.13}Cr_{0.22}Mn_{1.32}Ni_{0.14}V_{0.31}Fe_{0.06}$ they amounted +0.68 and −0.36 H/M, or +58 and −39% of the reference value, respectively. Such discrepancies (also taking into account the highest spread of the reference and calculated data for H/M observed during regression analysis; see Fig. 3a) are, most probably, caused by the oversimplified model (Eq. (11)) not accounting non-linearity and the mixed effects of the different factors, as well as possible influence of additional factors not included in the consideration.

It is well known that the hydrogen sorption capacities of the metallic hydrides strongly depend on the size of the interstitials in the metal matrix and chemical nature of the elements in the vertexes of the interstitials [6]. Accordingly, the empirical modelling which accounts these factors only indirectly and considers their total effects ($V_M$ for the size of interstitials ignoring their kind and surrounding; average VEC and electronegativity for the chemical nature of the surrounding elements), may cause significant deviations

of the reference data and results of the empirical calculations.

The deviations between the observed/reference and calculated values of $\Delta G_H^\circ$ were found to also be too high amounting from –4 to +6 kJ mol $(H_2)^{-1}$ that corresponds to the deviations of the plateau pressures (Eq. (9)) up to more than two orders of magnitude.

Taking into account the above-mentioned, it can be concluded that the approach undertaken in this study has a limiting predicting capacity and allows only very rough quantitative estimations. Nevertheless, we consider it as quite useful since it allows us to estimate the contribution of each key property of multi-component hydrogen storage alloys into their main hydrogen sorption performances. As it was shown the previous sections, the most significant factors relate to the structure (type and unit cell volume) and chemical nature of the alloy components (VEC, electronegativity) while the effect of other properties related to LEAs, MEAs and HEAs themselves (first of all, $\Delta S_{mix}$) remains minor if not negligible (Fig. 4). This finding is in line with our earlier conclusion [16] that hydrogen storage performances of the low-medium- and high-entropy alloys are rather similar[4], and thus hydride-forming HEAs might be considered as a group of conventional hydrogen storage alloys rather than their separate class.

Presently, we continue analysis of interrelation between the key properties and hydrogen sorption performance of the multi-principal component alloys, by applying advanced supervised machine learning models including decision tree and random forest ones. Though results of this study will be published later, preliminary findings showed that prediction capacity of the applied models is similar to the one reported in this article, with better adequacy of the random forest model.

On our opinion, further studies in this direction should be focused on the detailed analysis of the entries characterized by the maximum deviations of the observed / reference data from the calculated trend line that will assist one to reveal additional factors impacting hydrogen storage properties of hydrogen storage materials and, in turn, to create a reliable guiding tool for the selection or purposeful development of efficient materials for hydrogen and metal hydride energy technologies.

[4] Certainly, it relates only to the properties (H/M, $T_H$ and $\Delta G_H^\circ$) considered in this work. Other properties of hydrogen—metal systems including hysteresis and plateau slope may exhibit certain correlations with the key properties of HEAs. However, analysis of these correlations is not possible now, due to the lack of the corresponding reference data.

## CONCLUSIONS

• Machine learning-assisted study of the low-medium- and high-entropy hydrogen storage alloys, which crystallize in BCC, C14- and C15-$AB_2$, and $AB_5$ structures, has been conducted by linear regression analysis of the multi-factor correlation between the key properties of the alloys (mixing entropy and enthalpy, size and electronegativity mismatches, average valence electron concentration, unit cell volume per the metal atom) and their hydrogen sorption properties including hydrogen-to-metal atomic ratio, equilibrium temperature and the standard Gibbs free energy of hydrogenation.

• Comparison of the linear regression analysis results with additional reference and experimental data has shown that the applied model exhibits good qualitative correspondence with the reference data but has a limiting predicting capacity and allows only rough quantitative estimations.

• Based on sensitivity analysis, it was concluded that the unit cell volume, valence electron concentration, and, to a lesser extent, electronegativity mismatch, exhibit strong effects on the hydrogen sorption properties. The influence of other factors including the mixing entropy is minor if not negligible.

• Further machine learning studies of the low-medium- and high-entropy hydrogen storage alloys, including application of advanced supervised machine learning algorithms, should be focused on the detailed analysis of the entries characterized by the maximum deviations of the observed/reference data from the calculated trend that will allow one to reveal additional factors impacting hydrogen storage properties of hydrogen storage materials and, in turn, to create a reliable guiding tool for the selection or purposeful development of efficient materials for hydrogen and metal hydride energy technologies.

## FUNDING

The study of high entropy hydrogen storage alloys undertaken by the South African co-authors of this article (task statement, general methodology, collection of the reference data) was supported by the South African Department of Science and Innovation (DSI), within HySA Program, Key Project KP6-01.

Elaborating details and application of the calculation procedure, along with experimental verification of the calculation results were carried out by the Russian co-authors of this article funded by the Ministry of Science and Higher Education of the Russian Federation (Megagrant, Agreement no. 075-15-2022-1126, signed on July 1, 2022).

## CONFLICT OF INTEREST

The authors of this work declare that they have no conflicts of interest.

## REFERENCES


1. Filippov, S.P. and Yaroslavtsev, A.B., *Russ. Chem. Rev.*, 2021, vol. 90, p. 627.
2. Amirthan, T. and Perera, M.S.A., *J. Nat. Gas Sci. Eng.*, 2022, vol. 108, p. 104843.
3. Qureshi, F., Yusuf, M., Arham Khan, M., et al., *Fuel*, 2023, vol. 340, p. 127574.
4. Dornheim, M., Baetcke, L., Akiba, E., et al., *Prog. Energy*, 2022, vol. 4, p. 042005.
5. Lee, S.-Y., Lee, J.-H., Kim, Y.-H., et al., *Processes*, 2022, vol. 10, p. 304.
6. Hirscher, M., Yartys, V.A., Baricco, M., et al., *J. Alloys Compd.*, 2020, vol. 827, p. 153548.
7. Lototskyy, M.V., Tolj, I., Pickering, L., et al., *Prog. Nat. Sci.: Mater. Int.*, 2017, vol. 27, p. 3.
8. Lototsky, M.V., Davids, M.W., Fokin, V.N., et al., *Therm. Eng.*, 2024, vol. 71, p. 264.
9. Lototskyy, M.V., Tarasov, B.P., and Yartys, V.A., *J. Energy Storage*, 2023, vol. 72, p. 108165.
10. Yartys, V.A. and Lototskyy, M.V., *J. Alloys Compd.*, 2022, vol. 916, p. 165219.
11. Liu, J., Xu, J., Sleiman, S., et al., *Int. J. Hydrogen Energy*, 2021, vol. 46, p. 28709.
12. Joubert, J.-M., Paul-Boncour, V., Cuevas, F., et al., *J. Alloys Compd.*, 2021, vol. 862, p. 158163.
13. Sahlberg, M., Karlsson, D., Zlotea, C., and Jansson, U., *Sci. Rep.*, 2016, vol. 6, p. 36770.
14. Marques, F., Balcerzak, M., Winkelmann, F., et al., *Energy Environ. Sci.*, 2021, vol. 14, p. 5191.
15. Pedroso, O.A., Botta, W.J., and Zepon, G., *Int. J. Hydrogen Energy*, 2022, vol. 47, p. 32582.
16. Somo, T.R., Lototskyy, M.V., Yartys, V.A., et al., *J. Energy Storage*, 2023, vol. 73, p. 108969.
17. Rahnama, A., Zepon, G., and Sridhar, S., *Int. J. Hydrogen Energy*, 2019, vol. 44, p. 7337.
18. Rahnama, A., Zepon, G., and Sridhar, S., *Int. J. Hydrogen Energy*, 2019, vol. 44, p. 7345.
19. Suwarno, S., Dicky, G., Suyuthi, A., et al., *Int. J. Hydrogen Energy*, 2022, vol. 47, p. 11938.
20. Ahmed, A. and Siegel, D.J., *Patterns*, 2021, vol. 2, p. 100291.
21. Amiri, A. and Shahbazian-Yassar, R., *J. Mater. Chem. A*, 2021, vol. 9, p. 782.
22. Zhang, Y., Zhou, Y.J., Lin, J.P., et al., *Adv. Eng. Mater.,* 2008, vol. 10, p. 534.
23. Guruvidyathri, K., Vaidya, M., and Murty, B.S., *Scr. Mater.*, 2020, vol. 188, p. 37.
24. Stein, F. and Leineweber, A., *J. Mater. Sci.*, 2021, vol. 56, p. 5321.
25. Carroll, R., Lee, C., Tsai, C.-W., et al., *Sci. Rep.*, 2015, vol. 5, p. 16997.
26. Cheng, C.Y., Yang, Y.C., Zhong, Y.Z., et al., *Curr. Opin. Solid State Mater. Sci.*, 2017, vol. 21, p. 299.
27. Karlsson, D., Ek, G., Cedervall, J., et al., *Inorg. Chem.*, 2018, vol. 57, p. 2103.
28. Miracle, D.B. and Senkov, O.N., *Acta Mater.*, 2017, vol. 122, p. 448.
29. Pearson, W.B., *The Crystal Chemistry and Physics of Metals and Alloys*, New York: Wiley–Interscience, 1972.
30. Orimo, S., Nakamori, Y., Eliseo, J.R., et al., *Chem. Rev.*, 2007, vol. 107, p. 4111.
31. Andreasen, A., *Predicting Formation Enthalpies of Metal Hydrides*, Roskilde, Risø National Laboratory, 2004.
32. Davids, M.W., Martin, T.C., Fursikov, P.V., et al., *J. Phys.: Energy*, 2024, vol. 6, p. 035005.
33. Lototskyy, M.V., *Int. J. Hydrogen Energy*, 2016, vol. 41, p. 2739.
34. Yang, S., Han, S., Song, J., and Li, Y., *J. Rare Earths*, 2011, vol. 29, p. 692.
35. Dongliang, C., Chenglin, Z., Zhewen, M., et al., *Int. J. Hydrogen Energy*, 2012, vol. 37, p. 12375.
36. Casini, J.C.S., Guo, Z.P., Kun, LiuH., et al., *Trans. Nonferrous Met. Soc. China*, 2015, vol. 25, p. 520.
37. Ma, M., Sun, J., Fan, Y., et al., *J. Rare Earths*, 2015, vol. 33, p. 850.
38. Sun, J., Fan, Y., Liu, B., et al., *J. Alloys Compd.*, 2015, vol. 641, p. 148.
39. Zhou, W., Zhu, D., Wang, Q., et al., *Int. J. Hydrogen Energy*, 2015, vol. 40, p. 10200.
40. Casini, J.C.S., Silva, F.M., Guo, Z., et al., *Int. J. Hydrogen Energy*, 2016, vol. 41, p. 17022.
41. Zhou, W., Wang, Q., Zhu, D., et al., *Int. J. Hydrogen Energy*, 2016, vol. 41, p. 14852.
42. Zhou, W., Zhu, D., Tang, Z., et al., *J. Power Sources*, 2017, vol. 343, p. 11.
43. Cao, J., Xie, H., Wen, Z., et al., *Int. J. Electrochem. Sci.*, 2017, vol. 12, p. 5854.
44. Zhou, W., Tang, Z., Zhu, D., et al., *J. Alloys Compd.*, 2017, vol. 692, p. 364.
45. Zhou, W., Zhu, D., Liu, K., et al., *Int. J. Hydrogen Energy*, 2018, vol. 43, p. 21464.
46. Wang, C.C., Zhou, Y.T., Yang, C.C., and Jiang, Q., *J. Power Sources*, 2018, vol. 398, p. 42.
47. Kazakov, A.N., Blinov, D.V., Bodikov, V.Y., et al., *Int. J. Hydrogen Energy*, 2021, vol. 46, p. 13622.
48. Luo, L., Han, H., Feng, D., et al., *Renewables*, 2024, vol. 2, p. 138.
49. Chen, J., Huang, H., Xu, T., et al., *Int. J. Hydrogen Energy*, 2024, vol. 50, p. 1223.
50. Wijayanti, I.D., Denys, R., Suwarno, S., et al., *J. Alloys Compd.*, 2020, vol. 828, p. 154354.
51. Li, X., Li, B., Zhao, Y., et al., *J. Alloys Metall. Syst.*, 2023, vol. 2, p. 100006.
52. Pourarian, F. and Wallace, W., *Int. J. Hydrogen Energy*, 1986, vol. 11, p. 789.
53. Nygård, M.M., Ek, G., Karlsson, D., et al., *Acta Mater.*, 2019, vol. 175, p. 121.
54. Ek, G., Nygård, M.M., Pavan, A.F., et al., *Inorg. Chem.*, 2021, vol. 60, p. 1124.